BIOMARKERS FOR NEUROINFLAMMATION AND SATELLITE GLIA ACTIVATION IN DRY EYE DISEASE.

A THESIS

SUBMITTED TO THE FACULTY OF THE

UNIVERSITY OF MINNESOTA

BY

PANNAPORN STEPHENSON

IN PARTIAL FULFILMENT OF THE REQUIREMENTS

FOR THE DEGREE OF

MASTER OF SCIENE IN ORAL BIOLOGY

ADVISOR DR. DAVID A. BEREITER

OCTOBER 2018

ACKNOWLEDGEMENT

First, I would like to thank my advisor Dr. David A. Bereiter. His enthusiasm and knowledge in the topic have encouraged me to learn at an accelerated pace. I could not have imagined having a better mentor for my master's degree.

I also would like to express my gratitude to my committees, Dr. Carolyn Fairbanks and Dr. Kim Mansky. Without their valuable inputs, this thesis could not have been completed.

My sincere thanks also go to my lab mates, Mr. Randall Thompson and Dr. Mostafeezur Rahman, for troubleshooting my experiments and providing resources. Also, I thank Ms. Ann Hagen, assistant program director for helping me adjust to life in the United States.

Finally, I would like to thank my family and friends for providing me with continuous support throughout my years of study. This accomplishment would not have been possible without them.

ABSTRACT

Chronic dry eye (DE) is a burden to society with few effective treatments. Investigations of mechanisms for DE pain are limited by the lack of validated biomarkers and reliable measures of nocifensive behavior in an animal model.

To address these issues, we assessed eye wiping behavior and quantified qPCR and protein expression of Activating Transcription Factor 3 (ATF3) and Glial Fibrillary Acidic Protein (GFAP), as markers for neuronal injury and satellite glia activation, respectively, in the trigeminal ganglion (TG) of rat model of tear deficient DE.

Eye wipe behavior increased in males and females by 14 days after exorbital gland removal. Protein levels for ATF3 increased by 14d in females, but not in males, while GFAP increased in both sexes. By contrast, mRNA levels for ATF3 and GFAP did not change significantly in either sex. GFAP increases in protein were confirmed by immunohistochemistry as seen by an increase in the number of positively stained cells. The increase in GFAP was associated with an increase eye wipe behavior at 14d. These data suggested that neuron-glial mechanisms that mediate DE pain were different in males and females.

We conclude that GFAP, but not ATF3, is a valid biomarker for peripheral sensitization in this rat model of DE.

TABLE OF CONTENTS

LIST OF TABLES

LIST OF FIGURES

LIST OF ABBREVIATIONS

AM	=	ante meridiem
ANOVA	=	analysis of variance
ARVO	=	The Association for Research in Vision and Ophthalmology
ATF3	=	activating transcription factor 3
BAC	=	benzalkonium chloride
BCA	=	bicinchoninic acid
BrdU	=	bromodeoxyuridine
cDNA	=	complimentary deoxyribonucleic acid
DE	=	dry eye
EDTA	=	ethylenediaminetetraacetic acid
g	=	gram
GAPDH	=	glyceraldehyde 3-phosphate dehydrogenase
GFAP	=	glial fibrillary acidic protein
GS	=	glutamine synthetase
i.p.	=	intraperitoneally
IANX	=	inferior alveolar nerve injury

Ig	=	Immunoglobulin
IR	=	immunoreactivity
M	=	molar
mg/kg	=	milligram per kilogram
mm	=	millimeters
mM	=	millimolar
mOsm	=	milliosmoles
mRNA	=	messenger ribonucleic acid
NaCl	=	sodium chloride
^{o}C	=	degree Celsius
p	=	p value
PBS	=	Phosphate-buffered saline
pH	=	power of hydrogen
PHS	=	Public Health Service Policy
qPCR	=	quantitative polymerase chain reaction
RNA	=	ribonucleic acid
SDHA	=	succinate dehydrogenase subunit A
SEM	=	standard error of the mean

SG	=	satellite glia
TBS	=	tris-buffered saline
TBST	=	tris-buffered saline with 0.1% tween 20
TG	=	Trigeminal ganglia
TRPM8	=	Transient receptor potential cation channel subfamily M member 8
TRPV1	=	Transient receptor potential cation channel subfamily V member 1
vs	=	versus
µl	=	microliters
µg	=	micrograms

CHAPTER 1

INTRODUCTION

Dry eye (DE) is a multifactorial disease of the ocular surface often associated with debilitating pain and discomfort [1], [2], [3]. DE is known for its high prevalence in 5-50% of the population [4], [5], that increases with age and is greater in women than men at all age groups [6]. The chronic nature of DE places a substantial burden on patients and society [7], [8], [9]. Despite the well-calculated economic cost of DE, the mechanisms underlying pathophysiology of DE are still largely unknown [2]. No known effective treatments are available for more severe cases of DE [10].

The least manageable and most perplexing symptom of DE is burning pain which is felt primarily on the eye surface [11]. The eye surface consists of cornea, conjunctiva and eyelids. They are exposed to the environment; therefore, dutifully sense mechanical touch, temperature and osmolarity to maintain integrity and function of the eye [12], [13], [14], [15]. The cornea draws considerable attention and is often studied because of its high innervation density and sensitivity to external stimuli [16]. Cornea innervation stems from 50-450 primary sensory neurons whose cell bodies reside in ophthalmic and maxillary parts of the trigeminal ganglion (TG) (see review: Belmonte et al. 2017 [17]). Those neurons can be grouped as polymodal, thermoreceptor and selective mechanoreceptors, identifiable by specific markers TRPV1, TRPM8 and Piezo2 respectively [12], [18], [19], [20]. Cornea innervating neurons send axons that are 30% A-delta and 70% c-fibers via nasociliary branch of ophthalmic nerve and then long ciliary nerve [17]. Ciliary nerves branch extensively into stromal nerves to form subepithelial plexuses that project and divide further to form subbasal plexus before terminating near the ocular surface [16], [21]. Sensation of the

cornea eventually transmits toward second order neurons in the trigeminal brainstem nuclear complex and higher center in the brain.

The cornea is highly innervated consistent with its main function to protect the retina from damage by two protective reflexes: blink and tear production [22], [23], [24]. Since most corneal nerves are nociceptors, DE pain was long believed to be nociceptive pain induced by defective lacrimal functional unit [12], [25]. Therapeutic strategies to improve tear film quantity and quality, though adequate for mild DE, are not effective in severe DE [10].

Recently, investigators lean toward the concept that DE pain is neuropathic based on several lines of evidence. First, there is a poor correlation between corneal structural damage and pain intensity precluded tear film instability as the cause of DE pain [26], [27]. Second, direct nerve injury from refractive or cataract surgery resulted in DE-like pain [28], [29]. Third, In vivo corneal confocal microscopy in DE patients revealed increased tortuosity in subbasal plexus was correlated with pain intensity in clinic [30]. Fourth, DE has been shown to be comorbid with other pain syndromes, suggesting similar mechanisms [31]. Taken together, these arguments justify the revised definition of DE as "Dry eye is a multifactorial disease of the ocular surface characterized by a loss of homeostasis of the tear film, and accompanied by ocular symptoms, in which tear film instability and hyperosmolarity, ocular surface inflammation and damage, and neurosensory abnormalities play etiological roles." [1].

Induction of chronic ocular pain in DE likely involves sensitization of peripheral and central neurons, TG neurons supply the eye surface and are necessary for ocular pain sensation [16], [19], [32], [33]. Activated TG neurons can be identified metabolically by quantifying stress markers. Activating transcription factor 3 (ATF3) is a well-studied cellular stress marker that is inducible with a variety of cellular stressors, including infection and cancer [34], [35], [36], [37], [38], [39].

The expression of ATF3 increases in response to nerve injury after sensory nerve axotomy [40]. In the trigeminal sensory system, ATF3 increases significantly in an avulsion pain model [41] and after chronic constriction injury of the infraorbital nerve model [42].

Peripheral sensitization not only involves nociceptors producing more neuropeptides, but also coincides with functional and biochemical changes in sensory neurons [43]. The cell bodies of primary sensory neurons are surrounded by peripheral glia called satellite glia (SG). Satellite glia have been shown to influence neuronal functions in normal and pathological conditions [44], [45], [46], [47], [48] through mechanisms such as increased gap junction formation, purinergic channels, inward rectifying potassium currents and cytokine release [44], [45], [49], [50], [51], [52], [53], [54]. The expression of glial fibrillary acidic protein (GFAP) is low to undetectable under normal conditions and is a widely accepted as marker for activated astrocytes in the central nervous system and for activated SG in the periphery [45]. However, GFAP expression in the peripheral nervous system is not unique to SGs but is also expressed by Schwann cells [55], [56]. To ensure specificity of GFAP immunoreactivity in SG, counterstaining with a prominent SG marker like glutamine synthetase (GS) is warranted [42].

CHAPTER 2

HYPOTHESIS

The main hypothesis of this project is that that satellite glia activation contributes to ocular hyperalgesia in a rat model for dry eye. It is predicted that biological markers for satellite glia activation will correlate to the magnitude of nocifensive behavior. It is further predicted that the magnitude of behavior and satellite glia activation in this dry eye model will demonstrate sex difference as observed in the clinic.

CHAPTER 3

METHODS

General Methods

A total of 75 (39 male and 36 female) adult Sprague-Dawley rats (Harlan, Indianapolis, IN, USA), weighing between 250-400 g were used. Data from 3 rats were excluded from RNA and protein analysis because of inadequate protein concentration. In compliance with the Institutional Animal Care and Use Committee of the University of Minnesota (Minneapolis, MN, USA), animals were housed in pairs and given free access to food and water. The housing environment is temperature controlled to 25ºC ± 2ºC with 12:12 hour dark/light cycle (light on at 7.00 AM). The guidelines were set by ARVO and the National Institutes of Health guide for the Care and Use of Laboratory Animal (PHS Law 99-158, revised 2015). All efforts were made to minimize animal suffering and the number of animals used.

Model: Exorbital Gland Removal

Under 3-5% isoflurane anesthesia, the rat skin anterior to the left and right ears was shaved. Approximately 6-8 mm vertical incisions were made over the masseter muscles to expose and remove the left and right exorbital lacrimal glands. The incision was closed with 5-0 chromic gut sutures (Ethicon US, Somerville, NJ, USA). For 0d rat, the test was done before exorbital gland removal, serving as naïve control. After surgery, Ketoprofen (25 mg/kg, intraperitoneally (i.p.)) was given as a single dose. Rats survived for 2 days (2d), or 14 days (14d) before testing.

Eye Wipe Behavior

Rats were placed in plexiglass chamber for 1-hour acclimation. Then, 25 µl of increasing concentrations of sodium chloride (NaCl) solution (0.15M, 0.5M, 1.0M) were applied topically to the left eye with a micropipette. Eye wipe behavior, defined as deliberate forelimb movement over the left eye, was measured for 5 minutes after saline application. To control for desensitization, the rats were allowed 30-minute interval between successive testing periods. Grooming and scratching were also observed during the test period, but these behaviors were not measured.

RNA and Protein Analysis

Under deep anesthesia with sodium pentobarbital (50 mg/kg, i.p.), rats were perfused transcardially with 50 ml phosphate buffered saline (PBS) followed by 50 ml of RNA stabilizing solution (700g Ammonium sulfate, 20mM EDTA, 25mM Sodium citrate, pH 5.2). The trigeminal ganglia (TG) was excised and kept frozen at -80ºC overnight. Left and right TG from the same animal were pooled together. Total RNA was extracted from 0d, 2d, and 14d rats using TRIzol Reagent (ThermoFisher Scientific, Waltham, MA, USA). cDNA was synthesized from 30 µl of total RNA sample using iScript cDNA Synthesis Kit (Bio-Rad Laboratories, Hercules, CA, USA). qPCR was performed in duplicate on 2 µl cDNA with DNA Engine Opticon 2 and Chromo 4 (Bio-Rad Laboratories, Hercules, CA, USA) using iQ SYBR Green Supermix (Bio-Rad Laboratories, Hercules, CA, USA). The polymerase reaction started at 95ºC denaturation for 3 minutes followed by 40 cycles of 95ºC for 10 s, 58.5ºC for 20 s, and 72ºC for 30 seconds. Data analysis was performed using Livak's Method ($2^{-\Delta\Delta C_T}$). ATF3 and GFAP mRNA levels were calculated after normalizing two housekeeping genes (GAPDH and SDHA) in each sample.

Primer sets were as followed: GAPDH: F: 5’-agacagccgcatcttcttgt-3’, R: 5’-cttgccgtgggtagagtcat-3’. SDHA: F: 5’-gcaggcccatcggtgttgct-3’, R: 5’-tgacaccacggcactcccca-3’. ATF3: F: 5’-cctgcagaaggagtcaga gaa-3’, R: 5’-cgttctgagcccggacgata-3’. GFAP: F: 5’-gcgaagaaaaccgcatcacc-3’, R: 5’-tttggtgtccaggctggttt-3’. Data are presented as relative mRNA units compared with that of 0d control. All samples were analyzed in a blinded manner.

Protein isolation from the remaining sample after RNA extraction was done according to TRIzol Reagent User Guide. The protein concentration was determined with Pierce BCA Protein Assay Kit (ThermoFisher Scientific, Waltham, MA, USA). The samples were heat denatured in Laemmli Sample Buffer (Bio-Rad Laboratories, Hercules, CA, USA) and samples containing 40 μg of protein were subjected to electrophoresis on 4-20% Mini-PROTEAN TGX Gels (Bio-Rad Laboratories, Hercules, CA, USA) and transferred onto a polyvinylidene difluoride membrane (Immobilon-FL, MilliporeSigma, Burlington, MA, USA). Following rinsing with Tris-buffered saline (TBS), the membrane was incubated in 50% ODYSSEY blocking buffer (LI-COR Biosciences, Lincoln, NE, USA) in TBS. The membrane was incubated overnight at 4ºC with mouse anti-β-actin monoclonal antibody (1:500, MAB8929, R&D Systems, Minneapolis, MN, USA), rabbit anti-ATF3 antibody (1:500, ab 87213, Abcam, Cambridge, United Kingdom), and chicken anti-GFAP (1:1,000, GFAP, Aves Lab, Tigard, OR, USA). The following secondary antibodies were used: Cy2-conjugated anti-chicken IgY raised in donkey (Jackson ImmunoResearch, West Grove, PA, USA), IRDye-680-conjugated goat anti-rabbit IgG (LI-COR Biosciences, Lincoln, NE, USA), and IRDye-800-conjugated goat anti-mouse IgG (LI-COR Biosciences, Lincoln, NE, USA). The signal was visualized with ChemiDoc MP (Bio-Rad Laboratories, Hercules, CA, USA). All antibodies were diluted in Tris-buffered saline with 0.1% Tween 20 (TBST). Band intensity was quantified using Fiji software and normalized to the β-actin signal. Data are presented as relative protein expression compared to the control (0d) level.

Immunohistochemistry

Rats were anesthetized with sodium pentobarbital (50 mg/kg, i.p.) and perfused transcardially with saline followed by 10% formalin (ThermoFisher Scientific, Waltham, MA, USA). Left and right TGs were excised, post-fixed overnight at 4ºC and then trimmed and divided into 3 pieces. Tissues from animals with the same condition were embedded in the same paraffin block. The block was sectioned at 6 μm on a microtome and every 10th section was collected for immunostaining.

Antigen retrieval of rehydrated slides was done by incubating with sodium citrate buffer (10mM Sodium Citrate, 0.05% Tween 20, pH 6.0) at 95-100ºC for 1 hour. Autofluorescence background was quenched by 5 minutes incubation with 0.1% sodium borohydride in distilled water. Slides were blocked in 5% normal donkey serum and 0.1% Triton X-100 for 1 hour, then incubated in the primary antibodies: chicken anti-GFAP antibody (1:1,000, GFAP, Aves Lab, Tigard, OR, USA), and either rabbit anti-ATF3 antibody (1:500, ab 87213, Abcam, Cambridge, United Kingdom) or rabbit anti-glutamate synthetase (GS) antibody (1:500, G2781, Sigma-Aldrich, St. Louis, MO, USA). The slides were counterstained with the following secondary antibodies: Cy 2-conjugated anti-chicken IgY raised in donkey (Code 703-225-155, Jackson ImmunoResearch, West Grove, PA, USA) and Cy 3-conjugated anti-rabbit IgG raised in donkey (Code 711-166-152, Jackson ImmunoResearch, West Grove, PA, USA). The slides were coverslipped in slow fade mounting media (ThermoFisher Scientific, Waltham, MA, USA) and examined under a fluorescence microscope (Olympus BX51, Olympus, Shinjuku, Tokyo, Japan). The images were analyzed using Fiji software. The percentage of TG neurons with ATF3-immunoreactivity (IR) or encircled with GFAP-IR was calculated, as well as the ratio between densitometry of GFAP-IR and GS-IR in each image.

Statistical Analyses

All values are expressed as mean ± SEM. Eye wipe behavior was assessed by one-way repeated measures analysis of variance (ANOVA) followed by paired-sample t test. The time course of expression of the target genes and proteins were analyzed using one-way ANOVA followed by independent two-sample t test assuming unequal variance. A value of $p < 0.05$ was defined as significant.

CHAPTER 4

RESULTS

There were no overt signs of ocular hyperemia or inflammation after surgery with normal weight gain in all rats. “0d” is defined as the condition before surgical removal of DE or naive control condition. All changes were measured against values obtained from 0d animals.

Eye Wipe Behavior

Ocular application of 0.15M NaCl did not induce eye wiping after exorbital gland removal (Figure 1A, light blue bars). Ocular application of 0.5M NaCl (~1,000 mOsm) also failed to induce eye pain behavior at 2d or 14d versus 0d (Figure 1A, blue bars, $F_{2,45}=2.2.5$, $p>0.1$), suggesting that 0.5M NaCl is below the threshold for inducing nociceptive behavior in this model. However, after 1.0M NaCl, there was highly significant increase in eye wipe behavior in 14d rats compared to controls ($p<0.001$). Eye wiping also was increased at 2d versus controls ($p<0.05$) and between 2d vs 14d rats ($p<0.01$) when males and females were assessed together (Figure 1A, dark blue bars). These data confirmed that eye wipe behavior is a reliable measure of nocifensive behavior in this rat model of aqueous-deficient dry eye. Although male and female rats displayed increases in eye wiping to 1.0M NaCl at 14d compared to 0d ($p<0.01$, Figure 1B), the time courses were different. In males, eye wiping to 1.0M NaCl was significant from controls only at 14d ($p<0.05$, Figure 1B, blue bars), whereas female rats showed increased eye wiping as early as 2 days after surgery ($p<0.05$, Figure 1B, pink bars).

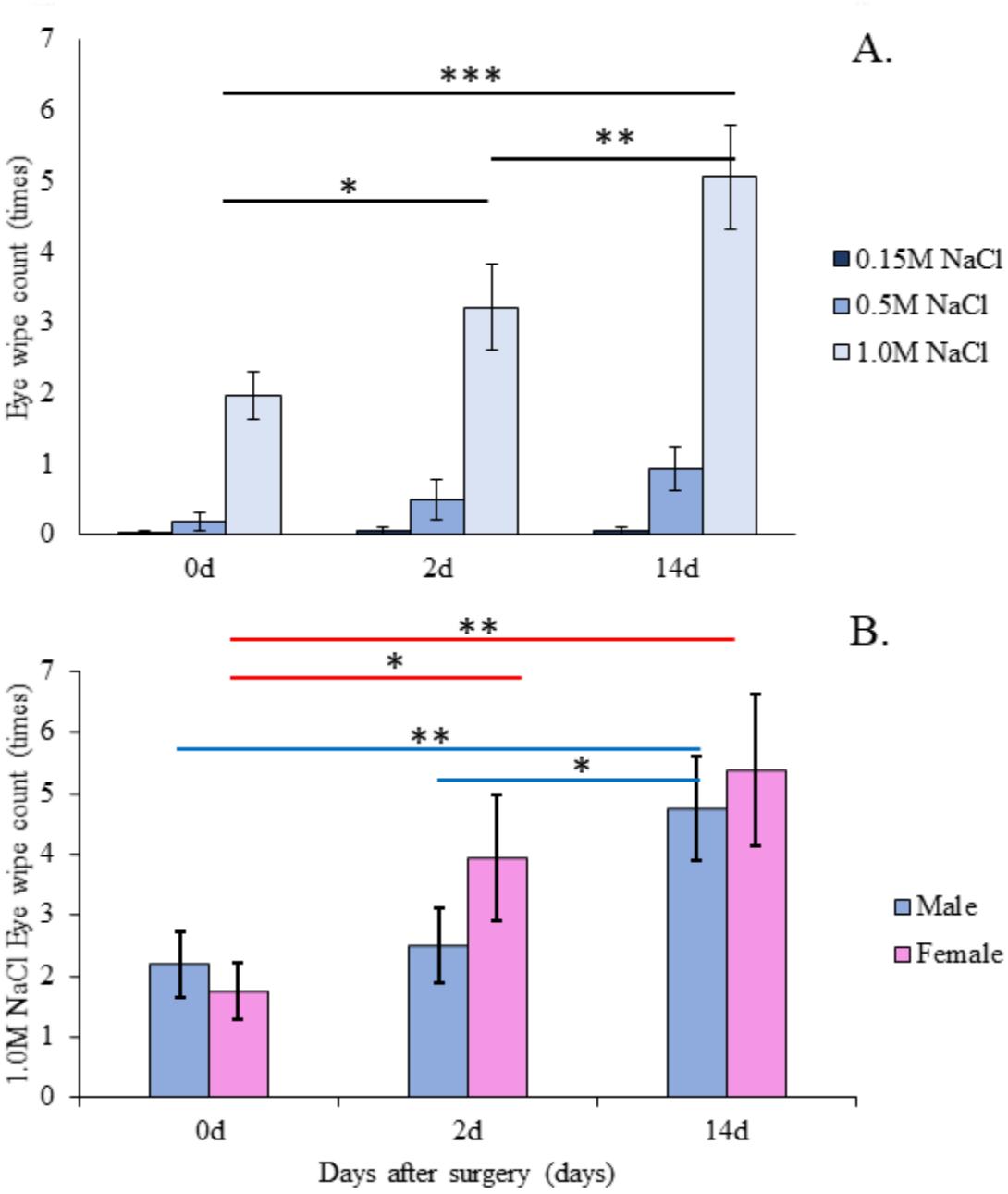

Figure 1. Eye wiping behavior response evoked by NaCl.

A. Eye wiping behavior count in response to escalating doses of NaCl at 0d, 2d and 14d after surgery (n=16).

B. Eye wiping behavior evoked by 1.0M NaCl in male (blue bars) and female (pink bars) at 0d, 2d, and 14d after surgery (n=8).

The data is presented as mean ± SEM. One-way ANOVA was used to determine if there was a difference between groups. Paired-sample t test was used to calculate p value between any two groups. * $p<0.05$, ** $p<0.01$, *** $p<0.001$.

RNA and Protein Analysis

Combined male and female TG samples from 0d, 2d and 14d DE rats expressed similar mRNA levels of ATF3 (Figure 2A, $F_{2,40} = 0.59$, $p>0.1$) and GFAP (Figure 2B, $F_{2,44} = 1.37$ $p>0.1$). When analyzed separately there were no sex differences in mRNA levels for ATF3 or GFAP (Figure 2C and 2D). When TG samples from males and females were assessed together ATF3 protein levels decreased at 2 days after surgery ($p<0.05$) and then increased at 14 days ($p<0.05$) compared to controls (Figure 3B). Similarly, analysis of GFAP protein levels from males and females combined were reduced at 2d ($p<0.01$) but increased at 14d ($p<0.01$, Figure 3C). However, when analyzed separately, statistically significant changes in ATF3 and GFAP protein levels were observed in female rats ($p<0.05$, Figure 3D and 3E, pink bars), but not in males.

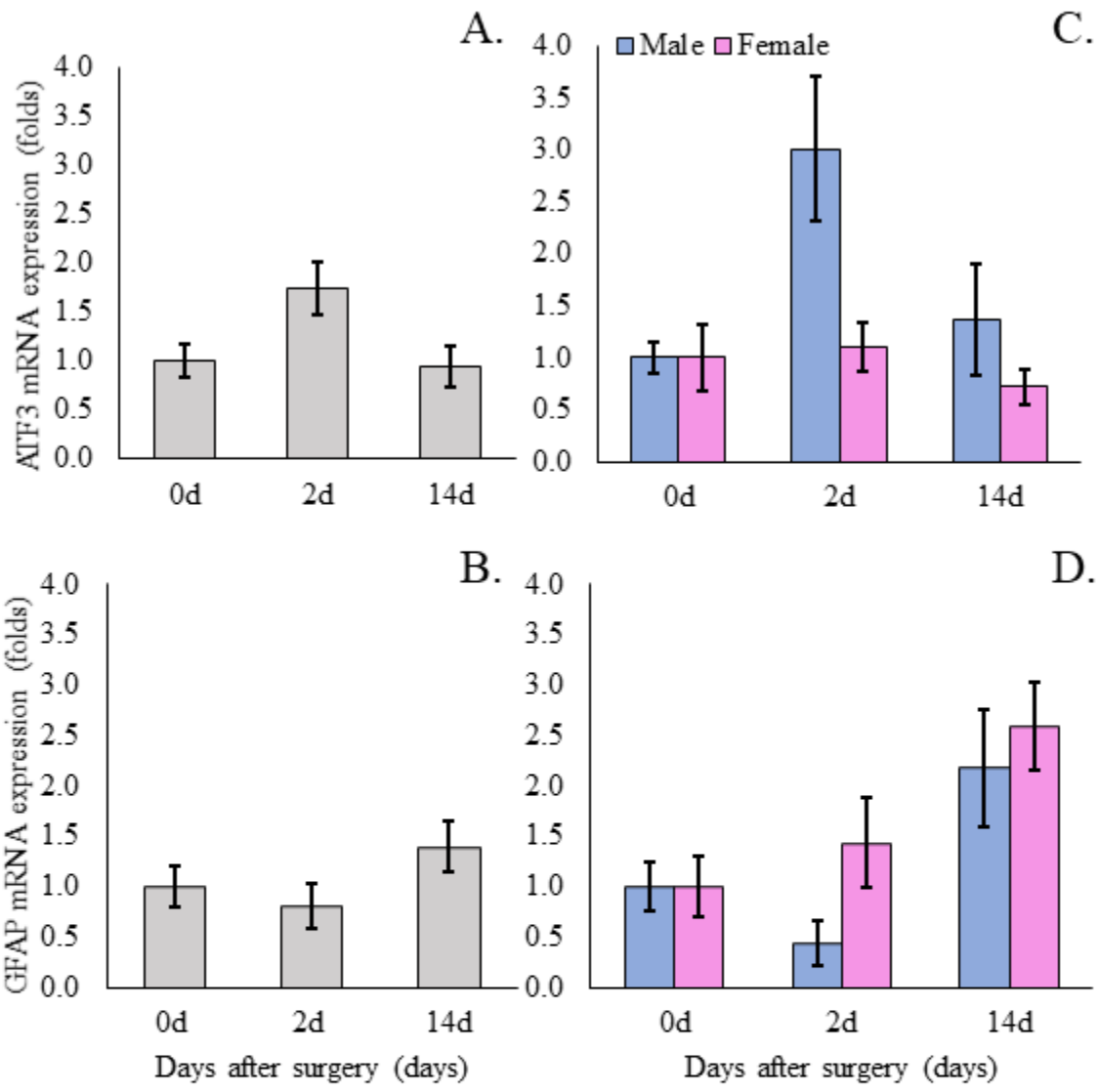

Figure 2. qPCR results from TG of 0d, 2d, 14d rats.

A. ATF3 mRNA expression over time in combined male and female animals (n=14-15/group).

B. GFAP mRNA expression over time in combined male and female animals (n=15-16/group).

C. ATF3 mRNA expression over time in male (blue bars, n=6-8/group) and female (pink bars, n=7-8/group) rats.

D. GFAP mRNA expression over time in male (blue bars, n=6-8/group) and female (pink bars, n=8/group) rats.

The data is presented as mean ± SEM. One-way ANOVA was used to determine if there was a difference between groups.

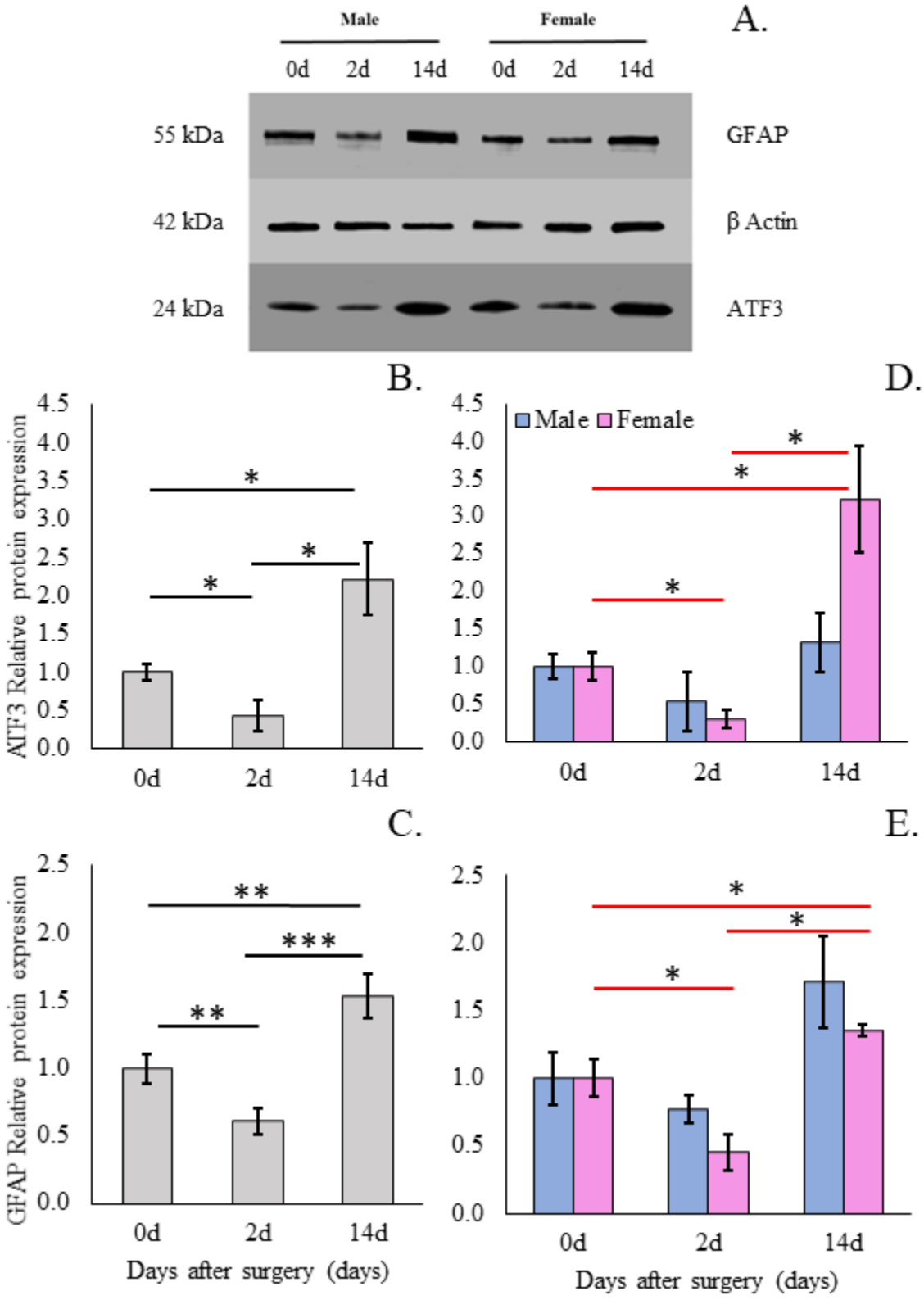
A.
Male
Female
0d
2d
14d
0d
2d
14d
55 kDa
GFAP
42 kDa
β Actin
24 kDa
ATF3
B.
ATF3 Relative protein expression
D.
Male
Female
C.
GFAP Relative protein expression
E.
Days after surgery (days)
Days after surgery (days)

Figure 3. Western blot results from TG of 0d, 2d, 14d rats (on previous page).

A. Example western blot data from 6 different animals (arranged by column; 3 left columns:male, 3 right columns:female) with 3 target proteins (arrange by row; top:GFAP, middle:β actin, bottom:ATF3).

B. ATF3 protein expression over time in combined male and female animals (n=8/group).

C. GFAP protein expression over time in combined male and female animals (n=8/group).

D. ATF3 protein expression over time in male (blue bars, n=4/group) and female (pink bars, n=4/group) rats.

E. GFAP protein expression over time in male (blue bars, n=4/group) and female (pink bars, n=4/group) rats.

The data is presented as mean ± SEM. One-way ANOVA was used to determine if there was a difference between groups. Independent-sample t test was used to calculate p value between any two groups. * $p<0.05$, ** $p<0.01$, *** $p<0.001$.

Immunohistochemistry

The ATF3 immunoreactive cells with a neuronal profile as a percentage of total TG cells was decreased at 2 days ($p<0.05$, Figure 4. right panels: A, B, and C and Figure 5A). A decrease in the ATF3 ratio was observed in female ($p<0.05$) but not in male rats (Figure 5D). Females displayed a greater percentage of ATF3 cells at 0d ($p<0.05$, Figure 5.D) but not at 2d or 14d. In contrast, the ratio GFAP-IR to total cells with a neuronal profile in TG increased after 2 days ($p<0.05$, Figure 4. middle panels: D, E and F and Figure 5B). When these data were assessed by sex, females displayed a higher percentage of GFAP-IR cells at 0d ($p<0.05$, Figure 5E, pink bars) and at 14 days ($p<0.01$), while males had a transient increase only at 2d ($p<0.05$, Figure 5E, blue bars. In females, GFAP-IR percentage resembled the western blot results with an initial decrease at 2d ($p<0.01$, Figure 5E, pink bars) and then an increase at 14d ($p<0.05$). When calculated as a percentage of GFAP-IR cells and ATF3-IR cells in the same image for males and females combined, there was an increase by 2d ($p<0.05$, Figure 5C) that reached a maximum value of 200% at 14d. The trend was consistent and detectable only in females (Figure 5F, pink bars).

Figure 6 demonstrated that GFAP-IR was detectable in cells with GS-IR, a general marker for SG cells. The increase in GFAP-IR was restricted to surrounding small diameter neurons (Figure 6A, B and C). Densitometry data for males and females combined revealed a delayed increase in ratio of GFAP-IR to GS-IR was observed (Figure 7A). However, when assessed by sex, although there was a sex difference at 0d and 2d ($p<0.05$, Figure 7B), the difference in GFAP-IR/GS-IR was detectable only in males (0d vs 14d and 2d vs 14d, $p < 0.01$, Figure 7B, blue bars) but not in females.

Figure 4. Example of ATF3 (red, A., D., and G.), GFAP (green, B., E. and H.) immunolabeling along with their combination (C., F. and I.) of TG samples of 0d (A. to C.), 2d (D. to F.) and 14d (G. to I.). (on next page)

J. The high magnification of TG from 14d male animal showing GFAP-IR cells surrounding neurons with no ATF3-IR (white arrows).

Scale bar for A. to I. = 200 μm (20x magnification), for J. = 50 μm (40x magnification).

Figure 5. Quantification of ATF3 and GFAP immunolabeling. (on previous page)

A. Percentage of cells with ATF3-IR to cells with neuronal profiles over time

B. Percentage of cells with GFAP-IR to cells with neuronal profiles over time.

C. Percentage of cells with GFAP-IR to cells with ATF3-IR over time.

D. Percentage of cells with ATF3-IR to cells with neuronal profiles over time in male (blue bars) and female (pink bars) rats.

E. Percentage of cells with GFAP-IR to cells with neuronal profiles over time in male (blue bars) and female (pink bars) rats.

F. Percentage of cells with GFAP-IR to cells with ATF3-IR over time in male (blue bars) and female (pink bars) rats.

For A. to C., no. of animal = 6/group, no. of section counted = 14-16/group. For D. to F., no of animals = 3/group, no. of section counted = 6-8/group.

The data is presented as mean ± SEM. One-way ANOVA was used to determine if there was a difference between groups. Independent-sample t test was used to calculate p value between any two groups. * $p<0.05$, ** $p<0.01$.

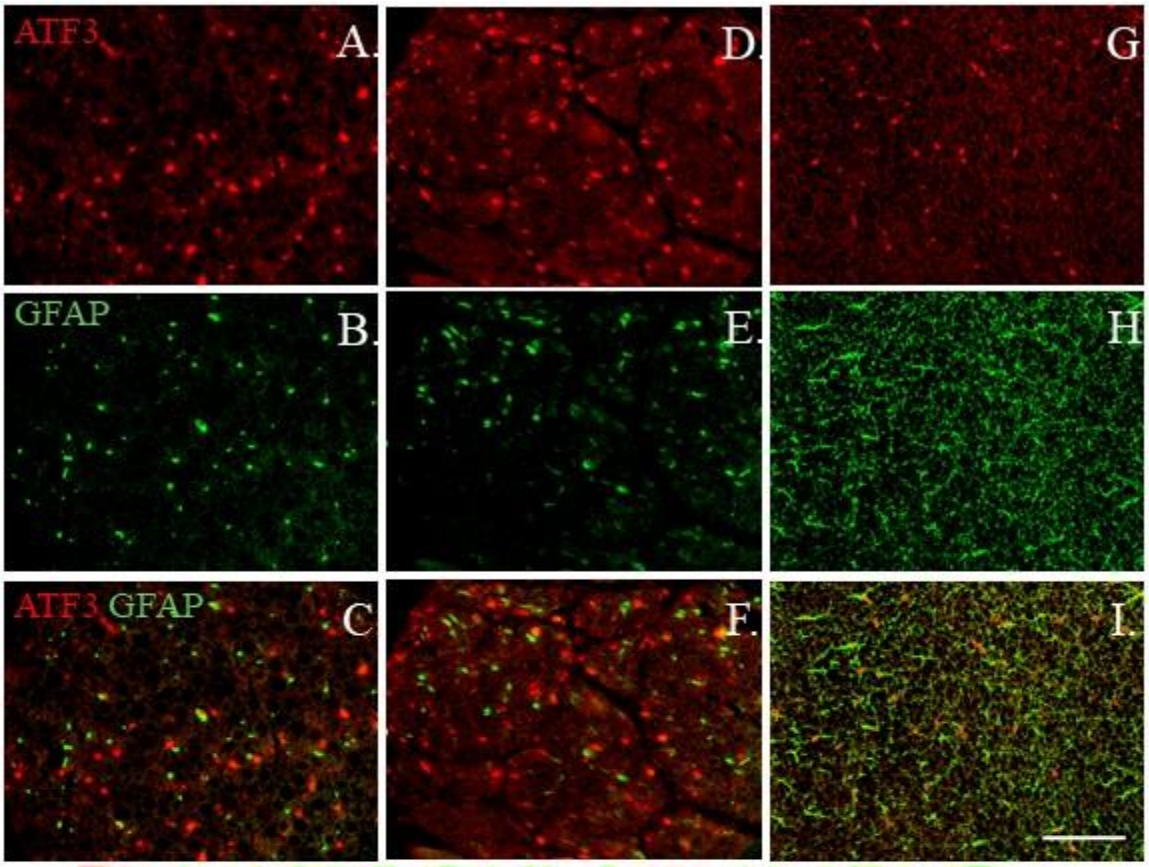

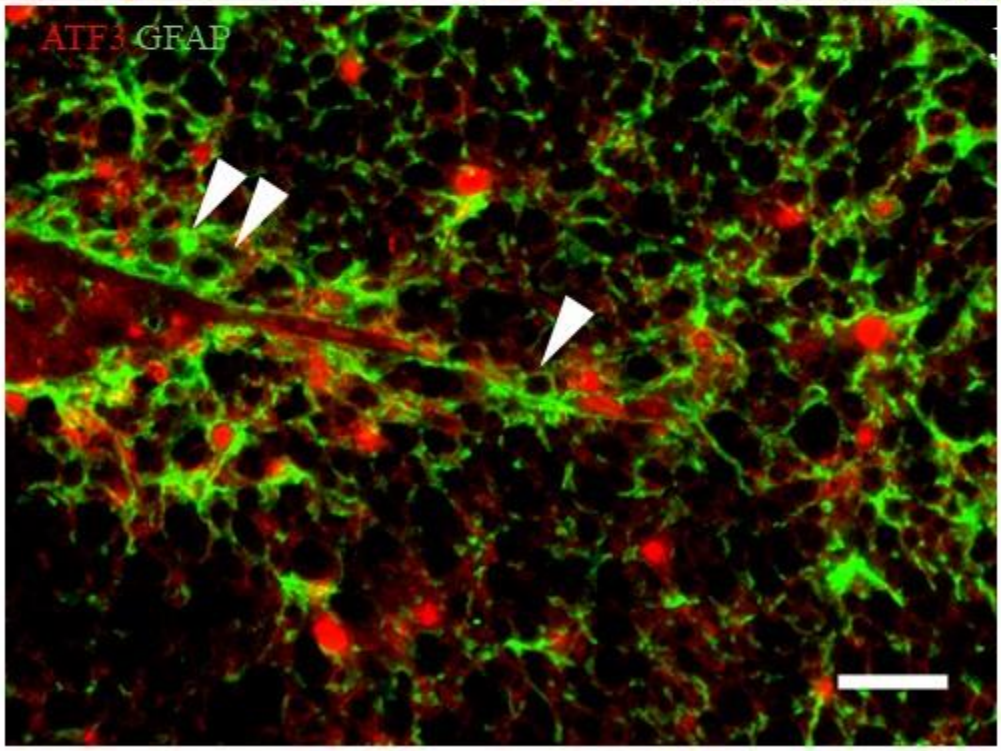

Figure 4. See description on previous page.

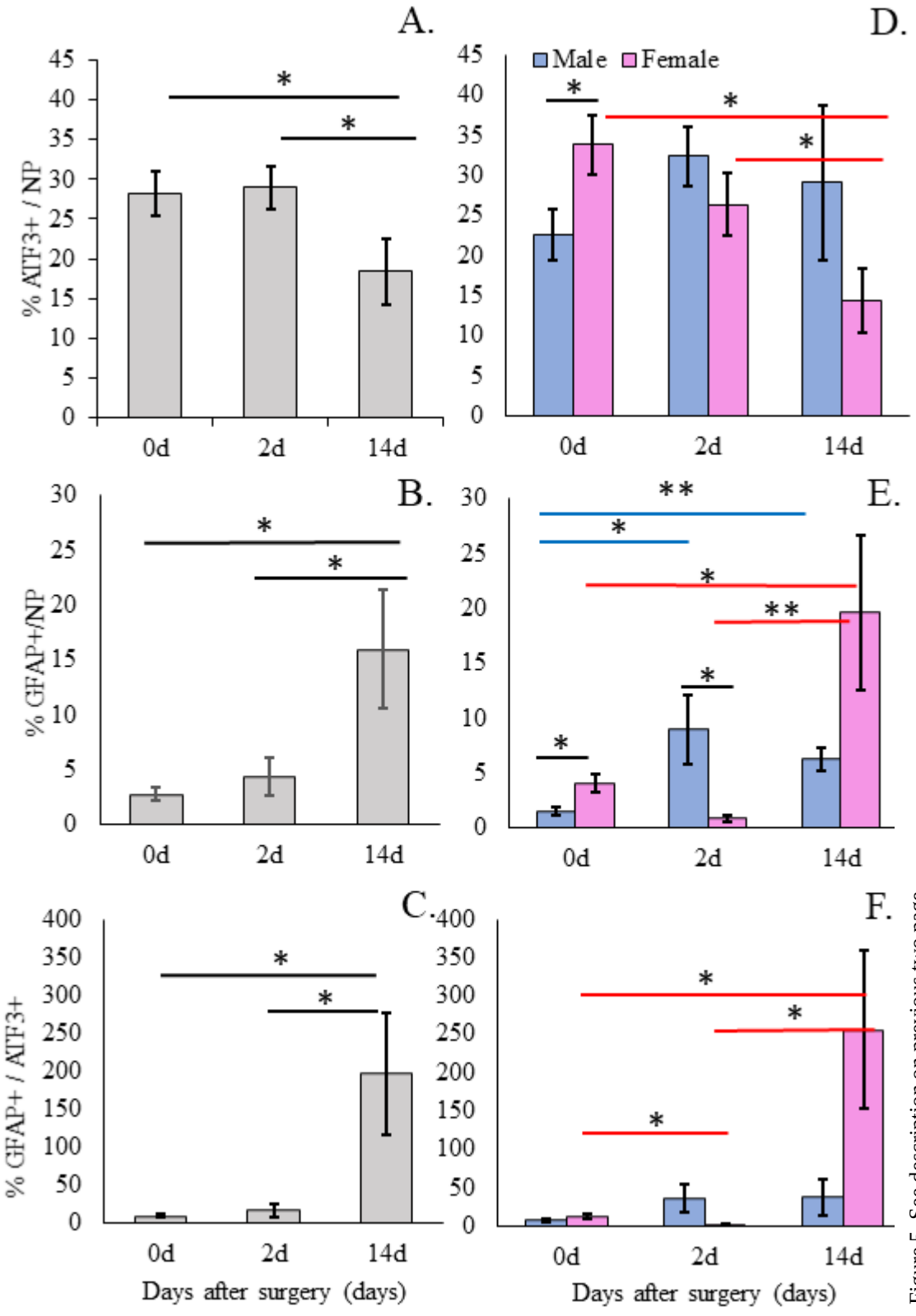

Figure 5. See description on previous two page.

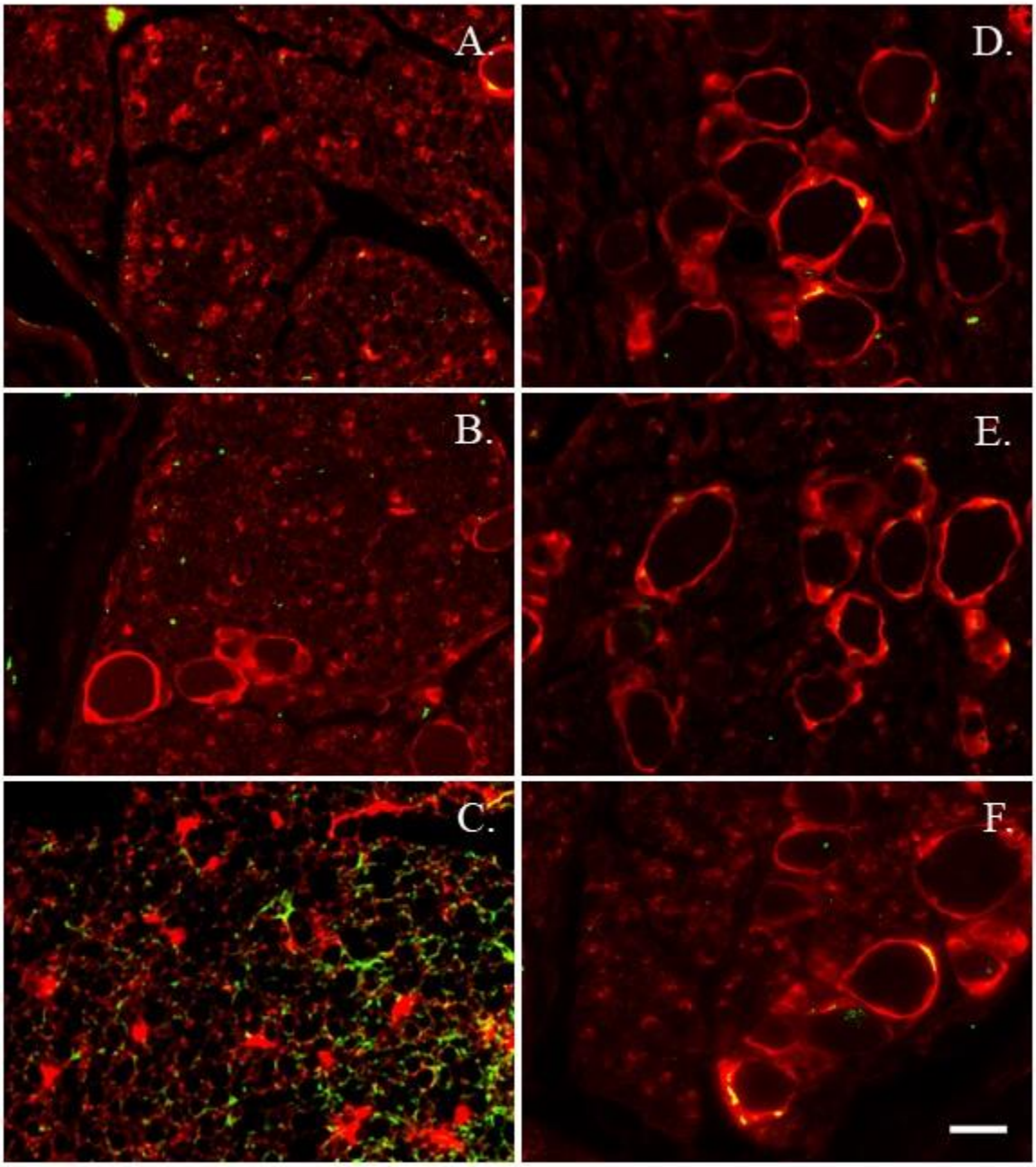

Figure 6. Example of GFAP immunoreactivity (green) counterstained with GS (red) at 40x magnification (scale bar = 100 um) with small diameter neurons (left: A. to C.) and large diameter neurons (right: D. to F.). The samples were collected at 0d (top: A. and D.), 2d (middle: B. and E.), 14d (bottom: C. and F.).

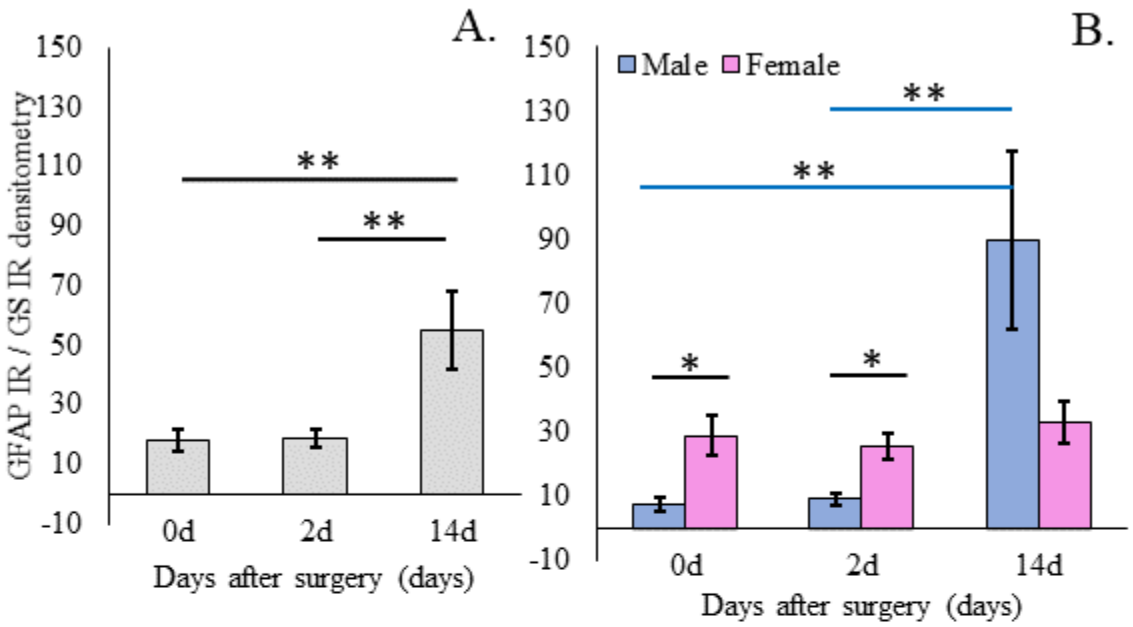

Figure 7. Quantification of GFAP and GS densitometry.

A. Percentage of ratio between area of GFAP-IR and area of GS-IR over time (no. of animal = 6/group, no. of section analyzed = 14-16/group).

B. Percentage of ratio between area of GFAP-IR and area of GS-IR over time in male (blue bars) and female (pink bars) rats (no of animals = 3/group, no. of section counted = 6-8/group).

The data is presented as mean ± SEM. One-way ANOVA was used to determine if there was a difference between groups. Independent-sample t test was used to calculate p value between any two groups. * $p<0.05$, ** $p<0.01$.

CHAPTER 5

DISCUSSION

Exorbital gland excision is a reliable model for tear-deficient dry eye and consistently, causes ~50% tear reduction at 14d after surgery [57], [65]. At 2 days after surgery (2d), the tear volume was assumed to be reduced, and although the corneal surface displayed no signs of inflammation, eye wiping behavior was increased. At 14 days after surgery (14d), exposing the eye surface to reduced tear volume for two weeks, results in irreversible and chronic inflammation of the ocular surface [57], [58]. Consequently, it is hypothesized that persistent ocular surface drying primes the sensory nerves to facilitate chronic ocular pain-like behavior. This experimental design allowed the behavioral and biochemical changes to ocular drying to be followed over time. Since DE is more prevalent in females than males it is necessary to include both sexes for appropriate data analysis.

Eye Wipe Behavior

The present study used a repeated analysis design to assess eye wiping behavior in the same animals over time to minimize the number of animals used and to strengthen the statistical analyses. The eye wipe test has been validated as a highly predictive facial pain behavior for both acute and chronic pain [59], [60], [61]. Hyperosmotic tears have been shown to correlate with increased inflammatory mediators and enhanced DE symptoms [62], [63]. Estimates of tear hyperosmolality in persistent DE patients may be as high as 800-1000 mOsm/kg [64]; however, NaCl concentrations restricted to the normal physiologic range did not induce eye wiping in our

model (Figure 1A, light blue bars). Although 2M to 5M NaCl solutions were needed to evoke eye wiping in awake animals in other studies [58], [59], [60], concentrations of NaCl as low as 0.5M did evoke increased orbicularis oculi electromyography in 14d DE animals compared to sham controls [65]. Therefore, we tested a range of concentrations from 0.15M, 0.5M to 1M NaCl and used 1M NaCl as a standardized stimulant to better distinguish between acute phase and chronic phase responses (Figure 1A). We found no increase in eye wipe counts in response to normal saline as seen in other studies [58]. Although other studies reported higher maximum eye wipe counts this may have been due to the use of higher NaCl concentrations (2-5 M NaCl). Another possible source of variation between this and other studies may be the definition of what constitutes eye wiping behavior. For example, Price et al. defined eye wiping as holding the eye tightly shut or actively grooming the face with either paw [61]. Importantly, previous studies of eye wiping in response to ocular instillation of stimulants only studied male animals. To the best of our knowledge, this study is the first to report sex differences in ocular nociceptive behavior in an animal model of DE. Figure 1B indicated that females either developed chronic eye pain sooner after exorbital gland removal and likely were more susceptible to hyperosmolar tears in DE. This basis for this difference in time course for the development of ocular sensitivity in males and females is not known.

RNA and Protein Analysis

The mRNA quantification did not reveal significant changes in ATF3 or GFAP levels over the 14d observation period (Figure 2). This may be due to the fact that this animal model did not inflict nerve injury directly as compared to nerve ligation or chemical burn models. Alternatively, it is possible that changes in mRNA expression occur transiently and return

towards baseline by 2d after surgery. Latremoliere et al. reported increased ATF3 and GFAP in addition to other cytokine genes [53]. In that study, ATF3 mRNA in TG rose immediately after infraorbital nerve chronic constriction injury, while GFAP mRNA increased initially then returned to baseline levels by 14 days. According to Launay et al., ATF3 mRNA in mice TG primary culture increased within 6 hours of benzalkonium chloride (BAC) treatment, whereas, after 7 days of BAC treatment ATF3 protein levels were not elevated [60]. Therefore, it is also possible that mRNA assessment of ATF3 and GFAP is not sensitive enough to observe changes in our model, since the increased in ATF3 mRNA may not correlate with increase in protein expression in tissue.

Western blot is a common method to quantify ATF3 protein levels in cell culture [34], [35], [36], but not necessarily in whole sensory ganglion tissues. Our data showed an initial decrease in ATF3 expression at 2d then a later increase by two-fold at 14d (Figure 3B). A similar pattern of expression was observed in GFAP with greater significance but of lower magnitude (Figure 3C). GFAP western blot had been done in extracephalic and cephalic pain studies [48], [50]. Nascimento et al. reported that GFAP increased in dorsal root ganglion neurons by day 4 and remained elevated for least 14 days in rat monoarthritic model [48]. For trigeminal pain, Kaji et al. demonstrated GFAP protein level doubled as early as 1 day and remained elevated up to 14 days after inferior alveolar nerve injury (IANX) compared to naïve condition [50]. Interestingly, IANX GFAP levels were different from sham controls only at day 8. This suggested that the sham operation influenced GFAP level and that increases in GFAP were not specific to neuronal damage.

Our data suggested a trend for sex differences in ATF3 and GFAP changes in females compared to males at all time points. This information has not been reported since previous studies used only male animals. Sex differences in ATF3 were investigated at the physiologic

level by Spinelli et al. [66]. That study showed that females had greater upregulation of ATF3 mRNA expression in lung tissue than male mice in an acute model of airway neutrophilia. Sex differences in GFAP level of astrocytes have been reported in several brain areas of multiple species, namely rat amygdala [67], hamster cerebellum [68], mice corpus callosum and optic tracts [69].

Immunohistochemistry

Figure 5A showed that the percentage of ATF3 positive cells decreased by 30% from baseline at 14d. Use of ATF3 as a maker for neuronal injury has not been consistent since one study reported no increase in ATF3 in TG after chemical injury [60], while others reported a 2-fold increase at 7 days in a monoarthritic model [48]. The ratio between GFAP positive and ATF3 positive cells in our study increased by 200% (Figure 5C), indicating that GFAP immunoreactivity was not limited to the surrounding of ATF3 positive cells. A similar result was reported by Donegan et al., in which only dividing SGs were detected surrounding ATF3 positive cells (GFAP colocalized with BrdU) [42].

In a study of the time course of ATF3 and GFAP protein expression, GFAP positive cells surrounding ATF3 negative neurons were found during the subacute phase of extraction pain model, while GFAP positive cells in chronic states were more likely to surround ATF3 positive neurons [41]. By contrast, we found that the increase in GFAP immunoreactivity coincided with a decrease in ATF3 immunoreactivity.

An increase in GFAP positive cells was expected since comparable results have been reported by several groups in other pain models [41], [42], [45], [48], [50]. The magnitude of increase in our study (5 to 15%) was different from that of Takeda et al. (10 to 30%), possibly because

Takeda studied fluorogold tagged TG neurons after direct nerve injury and only in male Wistar rats [45]. It is possible that the elevated GFAP can result from cell division or functional gain of satellite glia [42]. It will be important to determine if there was SG cell division to better characterize SG's role in this DE model.

Figure 6 demonstrated that GFAP was colocalized with GS, a widely-accepted universal SG marker. These data are consistent with that of Gunjigake et al. [41], precluding the plausible confounding GFAP signal from Schwann cells. Also, our data suggested that the increase in GFAP immunoreactivity was largely restricted to small diameter cells. This information agrees with data from Gunjigake et al. and Kaji et al. [41], [50].

Sex Differences in Chronic Pain

Sex differences in chronic pain sensation have been well-documented in clinical and preclinical studies and suggest that both biologic factors as well as socio-cultural contribute [70]. Considerable evidence has shown that both ascending nociceptive and descending inhibitory tracts within the CNS display sex differences. Marked sex differences were seen in the spared nerve injury (SNI) model in which male mice developed chronic pain via microglia activation and no T cell infiltration, while in females T cell infiltration alone was adequate to induce chronic pain [71]. Recently, Tran et al. reported that aromatase, an enzyme that converts androgen to estrogen, was expressed in neurons in lamina I and V of the spinal and medullary dorsal horn [72]. Interestingly, the majority of aromatase positive neurons co-expressed markers for inhibitory interneurons. Although the presence of aromatase was similar in males and females, it is not known if downstream pathways of aromatase activation relevant for nociception are similar in males and females. In the periphery, Lopes et al. suggested that there was no sex difference in

basic neurological structures at transcriptional levels, but rather adaptive immune cells were the key mediators of chronic pain [73]. The present data do not support this hypothesis as significant since SG activation in the TG were seen in males and females while ATF3 increased only in females in this model for DE.

Although Hirata et al. reported that $GABA_A$ receptors directly modulate neural activity of corneal-innervating neurons in trigeminal subnucleus caudalis, these experiments were only conducted in naïve male rats [74]. It also cannot be excluded that sex differences in pain processing occur at higher levels of the CNS since sex differences in μ-opioid receptor distribution have been reported in midbrain areas by Loyd et al. [75].

CHAPTER 6

CONCLUSION

In search of a suitable biomarker for peripheral components of DE hyperalgesia in our model, we found that ATF3 and GFAP protein levels in TG vary over time following exorbital gland removal in male and female rats. These data suggested that GFAP was a more reliable candidate biomarker for DE nocifensive behavior since western blot quantification of GFAP protein level was increased at 14d and corresponded to the pattern of change in eye wipe behavior. The GFAP increase was confirmed by two immunolabeling analyses: cell counting and densitometry of TG sections. In contrast, the ATF3 protein levels measured by western blot were increased, while the number ATF3-IR cells seen by immunolabelling was decreased.

The role of sex differences in DE pain likely is complex and involves many factors in addition to changes in sensory neuron activity. This project is novel in that it assesses sex differences in ocular nocifensive behavior and potential biomarker expression in an animal model for DE. These data suggested that sex differences in ocular nocicpetive behavior may be mediated by central as well as peripheral mechanisms. It will be important in future studies to consider if central glia or immune cells may mediate the sex differences in DE pain.

BIBLIOGRAPHY

1. Craig JP, Nichols KK, Akpek EK, Caffery B, Dua HS, Joo CK, et al. TFOS DEWS II Definition and Classification Report. Ocul Surf. 2017;15(3):276-83.

2. Bron AJ, de Paiva CS, Chauhan SK, Bonini S, Gabison EE, Jain S, et al. TFOS DEWS II pathophysiology report. Ocul Surf. 2017;15(3):438-510.

3. Mertzanis P, Abetz L, Rajagopalan K, Espindle D, Chalmers R, Snyder C, et al. The relative burden of dry eye in patients' lives: comparisons to a U.S. normative sample. Invest Ophthalmol Vis Sci. 2005;46(1):46-50.

4. Stapleton F, Alves M, Bunya VY, Jalbert I, Lekhanont K, Malet F, et al. TFOS DEWS II Epidemiology Report. Ocul Surf. 2017;15(3):334-65.

5. Sambursky R. Presence or absence of ocular surface inflammation directs clinical and therapeutic management of dry eye. Clin Ophthalmol. 2016;10:2337-43.

6. Ahn JH, Choi YH, Paik HJ, Kim MK, Wee WR, Kim DH. Sex differences in the effect of aging on dry eye disease. Clin Interv Aging. 2017;12:1331-8.

7. Yu J, Asche CV, Fairchild CJ. The economic burden of dry eye disease in the United States: a decision tree analysis. Cornea. 2011;30(4):379-87.

8. Clegg JP, Guest JF, Lehman A, Smith AF. The annual cost of dry eye syndrome in France, Germany, Italy, Spain, Sweden and the United Kingdom among patients managed by ophthalmologists. Ophthalmic Epidemiol. 2006;13(4):263-74.

9. Galor A, Levitt RC, Felix ER, Sarantopoulos CD. Understanding the true burden of dry eye disease. Expert Rev Ophthalmol. 2015;10(5):403-5.

10. Jones L, Downie LE, Korb D, Benitez-Del-Castillo JM, Dana R, Deng SX, et al. TFOS DEWS II Management and Therapy Report. Ocul Surf. 2017;15(3):575-628.

11. Kalangara JP, Galor A, Levitt RC, Felix ER, Alegret R, Sarantopoulos CD. Burning Eye Syndrome: Do Neuropathic Pain Mechanisms Underlie Chronic Dry Eye? Pain Med. 2016;17(4):746-55.

12. Belmonte C, Acosta MC, Gallar J. Neural basis of sensation in intact and injured corneas. Exp Eye Res. 2004;78(3):513-25.

13. Hirata H, Dallacasagrande V, Mizerska K, Ivakhnitskaia E, Rosenblatt MI. Ambient Air Currents Activate Corneal Nerves During Ocular Desiccation in Rats: Simultaneous Recordings of Neural Activity and Corneal Temperature. Invest Ophthalmol Vis Sci. 2018;59(10):4031-43.

14. Hirata H, Mizerska K, Marfurt CF, Rosenblatt MI. Hyperosmolar Tears Induce Functional and Structural Alterations of Corneal Nerves: Electrophysiological and Anatomical Evidence Toward Neurotoxicity. Invest Ophthalmol Vis Sci. 2015;56(13):8125-40.

15. Hirata H, Mizerska K, Dallacasagrande V, Rosenblatt MI. Estimating the Osmolarities of Tears During Evaporation Through the "Eyes" of the Corneal Nerves. Invest Ophthalmol Vis Sci. 2017;58(1):168-78.

16. Marfurt CF, Cox J, Deek S, Dvorscak L. Anatomy of the human corneal innervation. Exp Eye Res. 2010;90(4):478-92.

17. Belmonte C, Nichols JJ, Cox SM, Brock JA, Begley CG, Bereiter DA, et al. TFOS DEWS II pain and sensation report. Ocul Surf. 2017;15(3):404-37.

18. Alamri A, Bron R, Brock JA, Ivanusic JJ. Transient receptor potential cation channel subfamily V member 1 expressing corneal sensory neurons can be subdivided into at least three subpopulations. Front Neuroanat. 2015;9:71.

19. Ivanusic JJ, Wood RJ, Brock JA. Sensory and sympathetic innervation of the mouse and guinea pig corneal epithelium. J Comp Neurol. 2013;521(4):877-93.

20. Bron R, Wood RJ, Brock JA, Ivanusic JJ. Piezo2 expression in corneal afferent neurons. J Comp Neurol. 2014;522(13):2967-79.

21. He J, Bazan HE. Neuroanatomy and Neurochemistry of Mouse Cornea. Invest Ophthalmol Vis Sci. 2016;57(2):664-74.

22. Quallo T, Vastani N, Horridge E, Gentry C, Parra A, Moss S, et al. TRPM8 is a neuronal osmosensor that regulates eye blinking in mice. Nat Commun. 2015;6:7150.

23. Kaminer J, Powers AS, Horn KG, Hui C, Evinger C. Characterizing the spontaneous blink generator: an animal model. J Neurosci. 2011;31(31):11256-67.

24. Dartt DA. Neural regulation of lacrimal gland secretory processes: relevance in dry eye diseases. Prog Retin Eye Res. 2009;28(3):155-77.

25. Stern ME, Gao J, Siemasko KF, Beuerman RW, Pflugfelder SC. The role of the lacrimal functional unit in the pathophysiology of dry eye. Exp Eye Res. 2004;78(3):409-16.

26. Bron AJ, Tomlinson A, Foulks GN, Pepose JS, Baudouin C, Geerling G, et al. Rethinking dry eye disease: a perspective on clinical implications. Ocul Surf. 2014;12(2 Suppl):S1-31.

27. Sullivan BD, Crews LA, Messmer EM, Foulks GN, Nichols KK, Baenninger P, et al. Correlations between commonly used objective signs and symptoms for the diagnosis of dry eye disease: clinical implications. Acta Ophthalmol. 2014;92(2):161-6.

28. Levitt AE, Galor A, Weiss JS, Felix ER, Martin ER, Patin DJ, et al. Chronic dry eye symptoms after LASIK: parallels and lessons to be learned from other persistent post-operative pain disorders. Mol Pain. 2015;11:21.

29. Iglesias E, Sajnani R, Levitt RC, Sarantopoulos CD, Galor A. Epidemiology of Persistent Dry Eye-Like Symptoms After Cataract Surgery. Cornea. 2018;37(7):893-8.

30. Cruzat A, Pavan-Langston D, Hamrah P. In vivo confocal microscopy of corneal nerves: analysis and clinical correlation. Semin Ophthalmol. 2010;25(5-6):171-7.

31. Lee CJ, Levitt RC, Felix ER, Sarantopoulos CD, Galor A. Evidence that dry eye is a comorbid pain condition in a U.S. veteran population. Pain Rep. 2017;2(6):e629.

32. Marfurt CF, Kingsley RE, Echtenkamp SE. Sensory and sympathetic innervation of the mammalian cornea. A retrograde tracing study. Invest Ophthalmol Vis Sci. 1989;30(3):461-72.

33. ten Tusscher MP, Klooster J, Vrensen GF. The innervation of the rabbit's anterior eye segment: a retrograde tracing study. Exp Eye Res. 1988;46(5):717-30.

34. Miyazaki K, Inoue S, Yamada K, Watanabe M, Liu Q, Watanabe T, et al. Differential usage of alternate promoters of the human stress response gene ATF3 in stress response and cancer cells. Nucleic Acids Res. 2009;37(5):1438-51.

35. Hashimoto Y, Zhang C, Kawauchi J, Imoto I, Adachi MT, Inazawa J, et al. An alternatively spliced isoform of transcriptional repressor ATF3 and its induction by stress stimuli. Nucleic Acids Res. 2002;30(11):2398-406.

36. Gilchrist M, Thorsson V, Li B, Rust AG, Korb M, Roach JC, et al. Systems biology approaches identify ATF3 as a negative regulator of Toll-like receptor 4. Nature. 2006;441(7090):173-8.

37. Jadhav K, Zhang Y. Activating transcription factor 3 in immune response and metabolic regulation. Liver Res. 2017;1(2):96-102.

38. Thompson MR, Xu D, Williams BR. ATF3 transcription factor and its emerging roles in immunity and cancer. J Mol Med (Berl). 2009;87(11):1053-60.

39. Hackl C, Lang SA, Moser C, Mori A, Fichtner-Feigl S, Hellerbrand C, et al. Activating transcription factor-3 (ATF3) functions as a tumor suppressor in colon cancer and is up-regulated upon heat-shock protein 90 (Hsp90) inhibition. BMC Cancer. 2010;10:668.

40. Tsujino H, Kondo E, Fukuoka T, Dai Y, Tokunaga A, Miki K, et al. Activating transcription factor 3 (ATF3) induction by axotomy in sensory and motoneurons: A novel neuronal marker of nerve injury. Mol Cell Neurosci. 2000;15(2):170-82.

41. Gunjigake KK, Goto T, Nakao K, Kobayashi S, Yamaguchi K. Activation of satellite glial cells in rat trigeminal ganglion after upper molar extraction. Acta Histochem Cytochem. 2009;42(5):143-9.

42. Donegan M, Kernisant M, Cua C, Jasmin L, Ohara PT. Satellite glial cell proliferation in the trigeminal ganglia after chronic constriction injury of the infraorbital nerve. Glia. 2013;61(12):2000-8.

43. Gangadharan V, Kuner R. Pain hypersensitivity mechanisms at a glance. Dis Model Mech. 2013;6(4):889-95.

44. Huang LY, Gu Y, Chen Y. Communication between neuronal somata and satellite glial cells in sensory ganglia. Glia. 2013;61(10):1571-81.

45. Takeda M, Tanimoto T, Kadoi J, Nasu M, Takahashi M, Kitagawa J, et al. Enhanced excitability of nociceptive trigeminal ganglion neurons by satellite glial cytokine following peripheral inflammation. Pain. 2007;129(1-2):155-66.

46. Takeda M, Takahashi M, Matsumoto S. Contribution of the activation of satellite glia in sensory ganglia to pathological pain. Neurosci Biobehav Rev. 2009;33(6):784-92.

47. Poulsen JN, Larsen F, Duroux M, Gazerani P. Primary culture of trigeminal satellite glial cells: a cell-based platform to study morphology and function of peripheral glia. Int J Physiol Pathophysiol Pharmacol. 2014;6(1):1-12.

48. Nascimento DS, Castro-Lopes JM, Moreira Neto FL. Satellite glial cells surrounding primary afferent neurons are activated and proliferate during monoarthritis in rats: is there a role for ATF3? PLoS One. 2014;9(9):e108152.

49. Huang TY, Belzer V, Hanani M. Gap junctions in dorsal root ganglia: possible contribution to visceral pain. Eur J Pain. 2010;14(1):49 e1-11.

50. Kaji K, Shinoda M, Honda K, Unno S, Shimizu N, Iwata K. Connexin 43 contributes to ectopic orofacial pain following inferior alveolar nerve injury. Mol Pain. 2016;12.

51. Hanani M. Intercellular communication in sensory ganglia by purinergic receptors and gap junctions: implications for chronic pain. Brain Res. 2012;1487:183-91.

52. Takeda M, Takahashi M, Nasu M, Matsumoto S. Peripheral inflammation suppresses inward rectifying potassium currents of satellite glial cells in the trigeminal ganglia. Pain. 2011;152(9):2147-56.

53. Latremoliere A, Mauborgne A, Masson J, Bourgoin S, Kayser V, Hamon M, et al. Differential implication of proinflammatory cytokine interleukin-6 in the development of cephalic versus extracephalic neuropathic pain in rats. J Neurosci. 2008;28(34):8489-501.

54. Zhao YJ, Liu Y, Zhao YH, Li Q, Zhang M, Chen YJ. Activation of satellite glial cells in the trigeminal ganglion contributes to masseter mechanical allodynia induced by restraint stress in rats. Neurosci Lett. 2015;602:150-5.

55. Mancardi GL, Cadoni A, Tabaton M, Schenone A, Zicca A, De Martini I, et al. Schwann cell GFAP expression increases in axonal neuropathies. J Neurol Sci. 1991;102(2):177-83.

56. Ajima H, Kawano Y, Takagi R, Aita M, Gomi H, Byers MR, et al. The exact expression of glial fibrillary acidic protein (GFAP) in trigeminal ganglion and dental pulp. Arch Histol Cytol. 2001;64(5):503-11.

57. Joossen C, Lanckacker E, Zakaria N, Koppen C, Joossens J, Cools N, et al. Optimization and validation of an existing, surgical and robust dry eye rat model for the evaluation of therapeutic compounds. Exp Eye Res. 2016;146:172-8.

58. Meng ID, Barton ST, Mecum NE, Kurose M. Corneal sensitivity following lacrimal gland excision in the rat. Invest Ophthalmol Vis Sci. 2015;56(5):3347-54.

59. Farazifard R, Safarpour F, Sheibani V, Javan M. Eye-wiping test: a sensitive animal model for acute trigeminal pain studies. Brain Res Brain Res Protoc. 2005;16(1-3):44-9.

60. Launay PS, Reboussin E, Liang H, Kessal K, Godefroy D, Rostene W, et al. Ocular inflammation induces trigeminal pain, peripheral and central neuroinflammatory mechanisms. Neurobiol Dis. 2016;88:16-28.

61. Price TJ, Patwardhan A, Akopian AN, Hargreaves KM, Flores CM. Modulation of trigeminal sensory neuron activity by the dual cannabinoid-vanilloid agonists anandamide, N-arachidonoyl-dopamine and arachidonyl-2-chloroethylamide. Br J Pharmacol. 2004;141(7):1118-30.

62. Sullivan B. Challenges in using signs and symptoms to evaluate new biomarkers of dry eye disease. Ocul Surf. 2014;12(1):2-9.

63. Willshire C, Bron AJ, Gaffney EA, Pearce EI. Basal Tear Osmolarity as a metric to estimate body hydration and dry eye severity. Prog Retin Eye Res. 2018;64:56-64.

64. Liu H, Begley C, Chen M, Bradley A, Bonanno J, McNamara NA, et al. A link between tear instability and hyperosmolarity in dry eye. Invest Ophthalmol Vis Sci. 2009;50(8):3671-9.

65. Rahman M, Okamoto K, Thompson R, Katagiri A, Bereiter DA. Sensitization of trigeminal brainstem pathways in a model for tear deficient dry eye. Pain. 2015;156(5):942-50.

66. Spinelli A, Ortiz NF, Nicoleau M, Sinha U, Caruso CR, DiAngelo S, et al. Sex Dependent Role of Activating Transcription Factor 3 (ATF3) Expression In Modulating The Asthmatic Phenotype In An Acute Mouse Model Of Airway Neutrophilia. Faseb Journal. 2017;31.

67. Rasia-Filho AA, Xavier LL, dos Santos P, Gehlen G, Achaval M. Glial fibrillary acidic protein immunodetection and immunoreactivity in the anterior and posterior medial amygdala of male and female rats. Brain Res Bull. 2002;58(1):67-75.

68. Suarez I, Bodega G, Rubio M, Fernandez B. Sexual dimorphism in the hamster cerebellum demonstrated by glial fibrillary acidic protein (GFAP) and vimentin immunoreactivity. Glia. 1992;5(1):10-6.

69. Velosky AG, Tucker LB, Fu AH, Liu J, McCabe JT. Cognitive performance of male and female C57BL/6J mice after repetitive concussive brain injuries. Behav Brain Res. 2017;324:115-24.

70. Melchior M, Poisbeau P, Gaumond I, Marchand S. Insights into the mechanisms and the emergence of sex-differences in pain. Neuroscience. 2016;338:63-80.

71. Sorge RE, Mapplebeck JCS, Rosen S, Beggs S, Taves S, Alexander JK, et al. Different immune cells mediate mechanical pain hypersensitivity in male and female mice. Nat Neurosci. 2015;18(8):1081-+.

72. Tran M, Kuhn JA, Braz JM, Basbaum AI. Neuronal aromatase expression in pain processing regions of the medullary and spinal cord dorsal horn. J Comp Neurol. 2017;525(16):3414-28.

73. Lopes DM, Malek N, Edye M, Jager SB, McMurray S, McMahon SB, et al. Sex differences in peripheral not central immune responses to pain-inducing injury. Sci Rep. 2017;7(1):16460.

74. Hirata H, Okamoto K, Bereiter DA. GABA(A) receptor activation modulates corneal unit activity in rostral and caudal portions of trigeminal subnucleus caudalis. Journal of Neurophysiology. 2003;90(5):2837-49.

75. Loyd DR, Wang XY, Murphy AZ. Sex Differences in mu-Opioid Receptor Expression in the Rat Midbrain Periaqueductal Gray Are Essential for Eliciting Sex Differences in Morphine Analgesia. Journal of Neuroscience. 2008;28(52):14007-17.

APPENDIX 1. AUTOFLUORESCENCE QUENCHING PROTOCOL

Table 1. Summary of Autofluorescence Protocol with Sodium Borohydride (NaBH4).

Reference	Species: Tissues	Type (Fixatives)	Quenching Agents	Protocol	Note
Baschong et al., 2001	Human: Bone marrow, myocardium, Bovine: Cartilage	Fixed, paraffin embedded (4% formaldehyde or 2.5% glutaraldehyde)	Ammonia (NH_3)-ethanol, Sodium borohydride ($NaBH_4$), Sudan Black B	Right after rehydration, 70% ethanol + 0.25% NH_3. Ice-cooled freshly prepared MHB buffer supplemented with 10 mg/ml $NaBH_4$ for 40 min. wash, then 0.1% Sudan black in 70% alcohol 30 minutes.	Ammonia-ethanol works well with human bone marrow. Sudan Black is suitable for human myocardium. The combination of all three is most efficient on paraffin and frozen fixed in formaldehyde or glutaraldehyde.
Clancy and Cauller, 1998	Rat (Sprague-Dawley): Brain	Frozen, free floating (4% formaldehyde)	$NaBH_4$ 0.1%	Incubate 3 minutes – 4 hours in $NaBH_4$ 0.1-2.0% in PBS., sometimes repeat incubation with fresh solution.	$NABH_4$ reduces background by 30% in brain tissue. 3-minute incubation is enough to detect reduction in background but 30 minute or more incubation makes it difficult to mount the tissue.

Reference	Species: Tissues	Type (Fixatives)	Quenching Agents	Protocol	Note
Davis et al., 2014	Human: Liver, Mouse: lung	Frozen (human liver), Fixed, paraffin embedded (mouse lung, 10% formalin)	Eriochrome black T, Sudan black B, $NaBH_4$	10-minute incubation with 200 µl of one of these reagents: EBT 1.65%, Sudan black B 0.3% in ethanol, $NaBH_4$ 1 mg/ml in 1x TBS on ice.	$NaBH_4$ results in marked reduction of autofluorescence with no interference with other fluorophore channels, and it is moderately easy to prepare and moderately reproducible.
Gundhi and Khare, 2018	Human: Glioma, hepatocellular, lung/thyroid/renal cell carcinoma	Fixed, paraffin embedded (10% formalin)	$NaBH_4$, then crystal violet before antigen retrieval, and Sudan black B after secondary antibodies.	Freshly prepared 0.1% $NaBH_4$ in PBS, pH 7.4 for 2 changes (2.5 minutes each without in-between wash) then 0.5% crystal violet for 9 minutes. then PBS - 5 min wash (3 times). Final treated (after secondary) - 0.1% SBB in 70% ethanol for 5 minutes in the dark.	Triple drugs work best. The image quality is highly consistent and stable over 2 years.

Reference	Species: Tissues	Type (Fixatives)	Quenching Agents	Protocol	Note
Luquin et al., 2010	Rat (Wistar): Brain	Frozen, free floating (3.75% acrolein)	$NaBH_4$ 1% for 30 minutes, then 50% ethanol containing 0.3% H_2O_2	Vibratome section, pretreated with $NaBH_4$ 1% for 30 minutes under agitation, then mount the slide, incubate with 50% ethanol containing 0.3% H_2O_2 for 30 minutes before regular staining.	$NaBH_4$ eliminates tissue autofluorescence, while ethanol + H_2O_2 increases fluorescent detection.
Sun et al., 2010	Mouse (SAMP8): Brain	Fixed, paraffin embedded	$NaBH_4$	Pretreatment with 1% sodium borohydride, and/or including 0.5% Tween-20 in the secondary antibody solution.	The author recommended the use of 1% $NaBH_4$ pretreatment and adding 0.5% Tween-20 in the diluting solution for the secondary antibodies in the IHC protocol.
Kajimura et al., 2016	Human: Thymus (archival tissues of 40 to 60 years)	Paraffin embedded	NH_3 in 70% ethanol, 3% H_2O_2 in methanol, 1mg/ml $NaBH_4$, 2.0mM glycine,	After antigen retrieval, incubate tissue in NH_3 in 70% ethanol for 1 hour at room temperature, then wash with 50% ethanol for 10 min. Or 3% H_2O_2 in	Treatment with NH_3 and Sudan black B is particularly useful.

			0.3% Sudan black B in 70% ethanol	methanol before either primary or secondary antibodies for 15 minutes. Or 1mg/ml $NaBH_4$ on ice for 10 minutes 3 times. Or 2.0mM glycine at room temperature for 1 hour. Or after antibody incubation, 0.3% Sudan black B in 70% ethanol for 1 hour at room temperature.	

References

1. Baschong W, Suetterlin R, Laeng RH. Control of autofluorescence of archival formaldehyde-fixed, paraffin-embedded tissue in confocal laser scanning microscopy (CLSM). J Histochem Cytochem. 2001;49(12):1565-72.

2. Clancy B, Cauller LJ. Reduction of background autofluorescence in brain sections following immersion in sodium borohydride. J Neurosci Methods. 1998;83(2):97-102.

3. Davis AS, Richter A, Becker S, Moyer JE, Sandouk A, Skinner J, et al. Characterizing and Diminishing Autofluorescence in Formalin-fixed Paraffin-embedded Human Respiratory Tissue. J Histochem Cytochem. 2014;62(6):405-23.

4. Gandhi P, Khare R. A Unique Immunofluorescence Protocol to Detect Protein Expression in Vascular Tissues: Tacking a Long Standing Pathological Hitch. Turk Patoloji Derg. 2018;34(1):57-65.

5. Luquin E, Perez-Lorenzo E, Aymerich MS, Mengual E. Two-color fluorescence labeling in acrolein-fixed brain tissue. J Histochem Cytochem. 2010;58(4):359-68.

6. Sun A, Liu M, Bing G. Improving the specificity of immunological detection in aged human brain tissue samples. Int J Physiol Pathophysiol Pharmacol. 2009;2(1):29-35.

7. Kajimura J, Ito R, Manley NR, Hale LP. Optimization of Single- and Dual-Color Immunofluorescence Protocols for Formalin-Fixed, Paraffin-Embedded Archival Tissues. J Histochem Cytochem. 2016;64(2):112-24.